A Geometry-Based Method for Automatic Estimation of Winding Turns in EV Component Motors

Hyung-Il Park1 and Min-Mo Koo2*

¹Department of Convergence Technology Laboratory, Korea Electric Power Research Institute, Daejeon 34056, Republic of Korea ²Department of Purpose-Built Mobility Group, Korea Institute of Industrial Technology, Gwangju 61012, Republic of Korea

(Received 20 June 2025, Received in final form 9 July 2025, Accepted 11 July 2025)

Electric vehicle (EV) component motors are typically powered by a 12V low-voltage supply, requiring high current operation to deliver sufficient torque and output. Under such conditions, the number of winding turns critically influences key electrical parameters such as back electromotive force (EMF), inductance, and resistance. In particular, current-dominant environments make the system more sensitive to the number of turns. However, most motor design and analysis workflows still rely on manually specified turn counts, limiting both analytical precision and design automation. This study proposes a geometry-based algorithm for automatically estimating the number of winding turns using stator parameters. The method incorporates geometric features such as coil diameter, insulation thickness, and slot shape to enable accurate prediction of winding arrangement. Simulation results demonstrate strong agreement with actual winding configurations and show superior performance compared to conventional approaches in terms of computational efficiency and structural feasibility. These results are expected to support automated motor design workflows and improve the accuracy of electromagnetic performance evaluation.

Keywords: EV component motor, winding turn estimation, automated motor design, slot fill factor

1. Introduction

The rapid advancement of semiconductor technology has made multicore processors widely accessible. As a result, high-speed electromagnetic simulations are now feasible through PC cluster-based parallel computing, eliminating the need for costly high-performance computing infrastructure. This has led to the widespread adoption of analysis and design tools that support multicore and parallel processing, enabling simulations of electric machines that incorporate nonlinear magnetic properties and complex geometries with high fidelity [1]. In addition, multiphysics simulation techniques that account for both electromagnetic and structural phenomena have further enhanced the accuracy of electric machine modeling [2]. Building on these developments, research has increasingly focused on advanced optimization methods that treat geometry as a design variable, such as topology optimization [3].

Alongside these efforts, recent studies have investigated the effects of winding shape and slot fill factor on AC losses and mechanical vibration, particularly in high space factor and hairpin winding configurations [4, 5]. These studies aim to optimize performance assuming a given number of winding turns, but do not address how the turn count itself should be determined. While the turn count plays a central role in defining electromagnetic characteristics, only a few studies have attempted to predict it quantitatively based on the geometry of the motor and structural constraints.

Despite ongoing advances in modeling tools, most electromagnetic simulations still require manual input of key parameters such as the number of winding turns and winding resistance during preprocessing. These values often rely on engineering experience, which can introduce variability into simulation accuracy. For example, back electromotive force (EMF) and resistance increase linearly with turn count, while inductance increases proportionally to the square of the turn count [6]. As such, turn count significantly affects core performance metrics including torque, efficiency, and thermal behavior.

This issue is particularly critical in electric vehicle (EV)

©The Korean Magnetics Society. All rights reserved. *Corresponding author: Tel: +82-62-600-6230 Fax: +82-62-600-6219, e-mail: mmkoo@kitech.re.kr

component motors, which often operate under low-voltage, high-current conditions. These motors typically use a 12V supply, and even in EVs equipped with high-voltage batteries, subsystem motors often retain this low-voltage configuration. In such constrained environments, high current is required to achieve the necessary torque and power, making turn count not merely a numerical parameter, but a fundamental design factor that influences the electrical and thermal performance of the system [7, 8].

Fig. 1 illustrates the concept of slot fill factor by showing an empty slot (a), a partially filled slot (b), and a fully filled slot (c). Traditionally, the number of turns is estimated by dividing the effective slot area multiplied by a fill factor by the cross-sectional area of the conductor. The fill factor is typically obtained from prototype measurements or empirical standards [9]. However, this empirical approach does not always account for physical constraints in the actual winding space and may result in design errors. In practice, when the available slot area cannot accommodate the intended number of turns, designers face a trade-off: either reduce the number of turns while keeping the original conductor diameter or use thinner conductors to preserve the desired turn count. The former leads to reduced EMF and inductance, which can lower torque output; the latter increases resistance, thereby reducing efficiency and increasing heat generation.

Therefore, accurate turn estimation is not just a matter of parameter selection but a structural design challenge. A reliable, quantitative method for estimating turn count is essential for automating the design process and improving performance prediction, particularly in low-voltage, high-current applications. Despite its importance, systematic research on turn estimation remains limited. This study proposes an algorithm that predicts the number of winding turns based on geometric data from the stator, including the core, insulators, nozzles, and conductor diameter. The

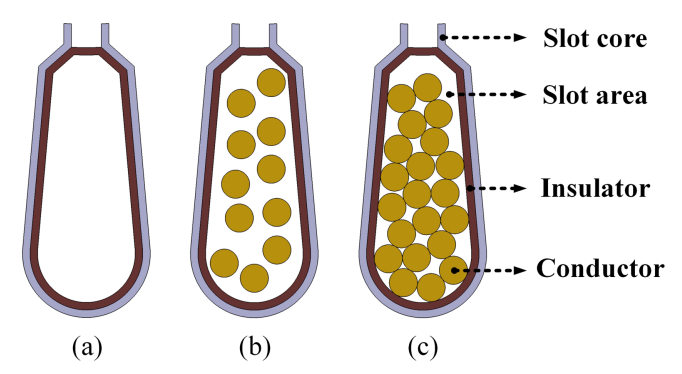


Fig. 1. (Color online) Conceptual diagram of the slot fill factor. (a) Empty slot, (b) Partially filled slot, (c) Fully filled slot.

algorithm models slot geometry and insulation layout to generate all necessary coordinates and parameters for estimating turn feasibility. It then evaluates whether the conductors can be placed without violating spatial boundaries or colliding with nozzle structures. A preliminary version of this work was presented at the Spring Conference of the Korean Society of Automotive Engineers in 2019 [1]. This paper expands upon that foundation by presenting the complete methodology, algorithm development, and comprehensive validation results.

2. Winding Constraints Based on Core Manufacturing Methods

The stator cores of small electric machines are generally manufactured using one of three methods: one-piece, segmented, or connected cores [10, 11]. Each method introduces distinct geometric constraints related to the insertion of winding nozzles and needles. These constraints define a geometric winding constraint region, where conductor placement is restricted, thereby limiting the usable winding area within the slot. Fig. 2 illustrates how these constraint regions and conductor layouts vary with core manufacturing methods. A one-piece core is formed by laminating steel sheets into a single circular structure, offering simplicity in fabrication. However, it imposes structural limitations: the minimum slot opening is determined by the wire diameter and the nozzle thickness. As a result, a portion of the slot becomes unusable, forming an invalid region that typically takes the shape of a rectangle with constant thickness perpendicular to the tangential direction of the outer back-yoke. A segmented core is assembled by winding each tooth individually before forming the complete stator. This approach enables

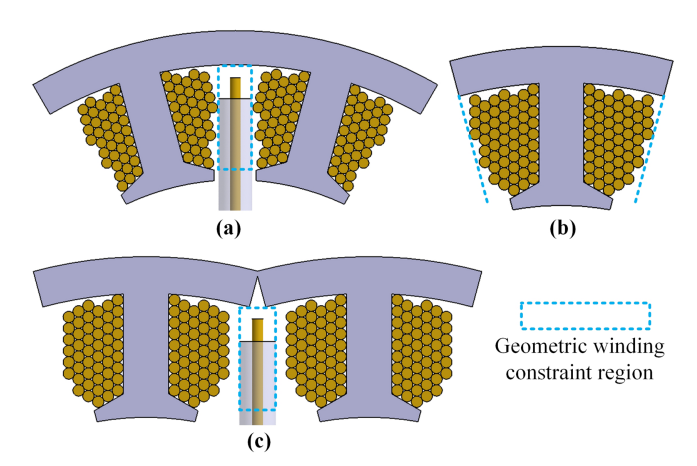


Fig. 2. (Color online) Geometric winding constraints based on core manufacturing methods: (a) One-piece core, (b) Segmented core, (c) Connected core.

full accessibility to the entire slot during winding. Aside from the insulation clearance between adjacent windings, no unusable region exists, allowing for maximum utilization of the slot area and eliminating slot opening constraints [12].

A connected core is manufactured in a linear configuration, with parallel-aligned teeth that are wound and then shaped into a circular stator through welding. Before circular forming, the fill factor is similar to that of linear machines, and the invalid slot region is rectangular and oriented perpendicular to the back-yoke. After shaping, this region transforms into a sector-shaped area perpendicular to the tooth, improving the fill factor. These structural advantages and limitations are discussed in more detail in [10, 12], which provide analyses based on practical applications and manufacturing considerations. Despite these structural characteristics, accurately predicting the number of winding turns remains difficult. This challenge arises because the required fill factor at the early design stage is often determined subjectively and based on the experience of the designer. To address this issue, the present study proposes a turn estimation method that accounts for the geometric constraints imposed by different core manufacturing methods. The method considers both the winding-available area and the physical limitations introduced during the manufacturing process.

3. Stator Geometry Modeling Framework

3.1. Variable Definitions

This study defines a set of geometric variables to model the stator core, insulators, and windings. Fig. 3 presents a schematic diagram illustrating the geometry and associated parameters of the stator slot. The proposed modeling approach is designed to be independent of the core manu-

 W_{so} W_{so} W

Fig. 3. (Color online) Definition of geometric variables and coordinate points used for stator modeling.

facturing method, allowing consistent variable definitions across different stator configurations.

In the case of a connected core, geometric interference between the winding nozzle and the back-yoke may occur if the back-yoke adopts an arc-shaped profile. To avoid this interference, it is common practice to design the interface between the tooth and the inner surface of the back-yoke as a perpendicular junction. Following this convention, the back-yoke in this study is modeled using a straight configuration, as shown in Fig. 3. The key variables used in this study are defined as follows:

 r_{so} : Outer radius of the stator

 r_{si} : Inner radius of the stator

 w_{so} : Half of the slot opening width

 h_{so} : Height of the slot opening

 w_t : Half of the tooth width

 N_s : Number of slots

 θ_{sh} : Shoe angle (interior angle between segments P_1 – P_2 and P_2 – P_3)

 r_{by} : Inner radius of the back-yoke

 t_{is} : Insulator thickness in the xy-plane d_{co} : Diameter of the bare copper wire

 t_{co} : Thickness of the coil coating

3.2. Two-Dimensional Stator Geometry Modeling

The stator geometry is modeled under the condition that the reference slot is aligned along the x-axis. To simplify the geometry, edge features such as chamfers and fillets are excluded, and all vertices are assumed to form sharp theoretical corners. Depending on the core modeling approach, the analytical formulation of the stator geometry may vary. In this study, the insulator is assumed to maintain a uniform thickness in all directions within the two-dimensional plane.

Fig. 4 shows the geometric reference points P_1 through

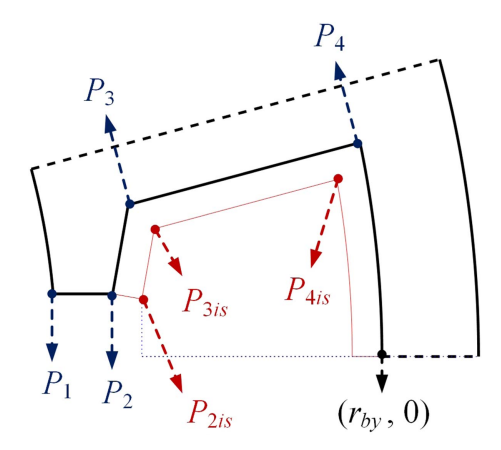


Fig. 4. (Color online) Geometric reference points used in modeling the stator core and insulator.

 P_4 used to define the stator core, along with corresponding insulator boundary points P_{2is} through P_{4is} . The coordinates of the stator geometry are derived from variables that define the height and width of the slot opening. Each reference point P_n in the xy-plane is represented as (x_n, y_n) . As shown in Fig. 4, the coordinates of P_1 and P_2 are given by Equation (1).

$$x_1 = \sqrt{r_{si}^2 - w_{so}^2} \tag{1.1}$$

$$y_1 = y_2 = w_{so} (1.2)$$

$$x_2 = x_1 + h_{so} (1.3)$$

The point P_3 , representing the inner vertex formed at the intersection between the tooth and the shoe, is determined by Equation (2), which incorporates the slot width and shoe angle.

$$x_{3} = \frac{\frac{w_{t} \sin \pi}{N_{s}} \tan \frac{\pi}{N_{s}} + x_{2} \tan \theta_{sh} + \frac{w_{t} \cos \pi}{N_{s}} + y_{2}}{\tan \theta_{sh} + \tan \frac{\pi}{N_{s}}}$$
(2.1)

$$y_3 = w_{so} - (x_3 - x_2) \tan \theta_{sh}$$
 (2.2)

The point P_4 , which marks the inner vertex at the intersection between the tooth and the back-yoke, can theoretically be derived from the coordinates of P_1 , P_2 , and P_3 . However, such a derivation requires complex trigonometric and geometric operations. To simplify the computation, the angle between P_4 and a reference point at $(\underline{r}_{by}, 0)$ is defined as shown in Equation (3).

$$\theta_4 = \frac{\pi}{N_s} - \sin^{-1} \left(\frac{w_t}{r_{by}} \right) \tag{3}$$

Using this angle θ_4 , the coordinates of P_4 are calculated using a standard polar-to-Cartesian transformation, as presented in Equation (4).

$$x_4 = r_{bv} \cos \theta_4 \tag{4.1}$$

$$y_4 = r_{bv} \sin \theta_4 \tag{4.2}$$

For a straight-type back-yoke configuration, the *x*-coordinate of the additional point P_5 is determined by Equation (5).

$$x_5 = x_4 + y_4 \tan \frac{\pi}{N_s} \tag{5}$$

The insulator is assumed to have a rectangular cross-

sectional profile. Accordingly, the starting point P_{2is} of the insulator is defined by translating the bottom vertex P_2 of the shoe in the normal direction by a distance equal to the thickness t_{is} of the insulator as shown in Equation (6).

$$x_{2is} = x_2 + t_{is} \cos\left(\theta_{sh} - \frac{\pi}{2}\right) \tag{6.1}$$

$$y_{2is} = y_2 - t_{is} \sin\left(\theta_{sh} - \frac{\pi}{2}\right) \tag{6.2}$$

The upper inner vertex P_{3is} of the insulator is derived by considering both the slope of the side of the shoe and the thickness of the insulator. Its coordinates are expressed analytically in Equation (7).

$$x_{3is} = \frac{x_{2is}T_{s1} - (x_3 + t_{is}\cos\theta_{3is})T_{s2}}{T_{s1} - T_{s2}} - \frac{y_{2is} - y_3 + t_{is}\sin\theta_{3is}}{T_{s1} - T_{s2}}$$
(7.1)

$$y_{3is} = (x_{3is} - x_{2is}) \tan(\pi - \theta_{sh}) + y_{2is}$$
 (7.2)

where
$$\begin{cases} T_{s1} = \tan(\pi - \theta_{sh}) \\ T_{s2} = \tan\left(\frac{\pi}{N_s}\right) \\ \theta_{3is} = \frac{\pi}{2} - \frac{\pi}{N_s} \end{cases}$$

The outer vertex of the insulator profile, P_{4is} , is given by Equation (8).

$$x_{4is} = \frac{-T_{s2}K_1 + \sqrt{4T_{s2}^2K_1^2 - 4(1 + T_{s2}^2)(K_1^2 - K_2^2)}}{2(1 + T_{s2}^2)}$$
(8.1)

$$y_{4is} = (x_{4is} - x_{3is})T_{s2} + y_{3is}$$
(8.2)

where
$$\begin{cases} K_1 = y_{3is} - T_{s2} x_{3is} \\ K_2 = r_{bv} - t_{is} \end{cases}$$

For the straight-type back-yoke configuration, the *x*-coordinate of the additional insulator point P_{5is} is calculated using Equation (9).

$$x_{5is} = T_{s2} y_{4is} + x_{4is} (9)$$

4. Turn Estimation Algorithm

Fig. 5 illustrates a conceptual diagram of a layer winding configuration within a stator slot. In the proposed algorithm, the first turn is placed at the position where the

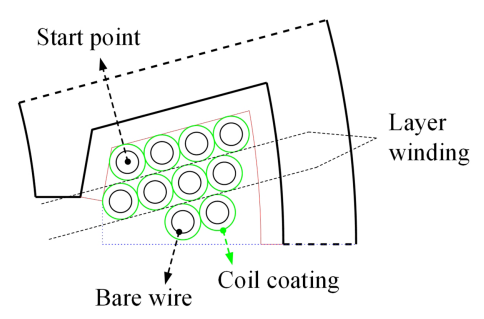


Fig. 5. (Color online) Conceptual illustration of initial conductor placement and layer winding configuration inside the slot.

conductor is simultaneously tangent to both the line segment connecting P_{2is} and P_{3is} and the segment connecting P_{3is} and P_{4is} , as shown in Fig. 5. The algorithm assumes that all conductors are arranged at uniform intervals and maintain mechanical contact with each other.

Fig. 6 compares conductor stacking configurations under different winding methods—random winding, layer winding, and orthocyclic winding—within the same slot [13]. Among these, orthocyclic winding is known for its high space efficiency, as upper-layer conductors are positioned to fill the grooves between lower-layer conductors, maximizing the slot fill. This method generally yields the highest fill factor among all known winding techniques. These stacking strategies reflect trade-offs in spatial efficiency, manufacturability, and coil arrangement complexity. Each winding method exhibits distinct characteristics in terms of conductor alignment and packing density, all of which influence machine performance in different ways. These characteristics and trade-offs are discussed in greater detail in [9, 13, 14]. However, in the machine considered in this study, the conductor diameter is relatively large, and the number of turns per slot is

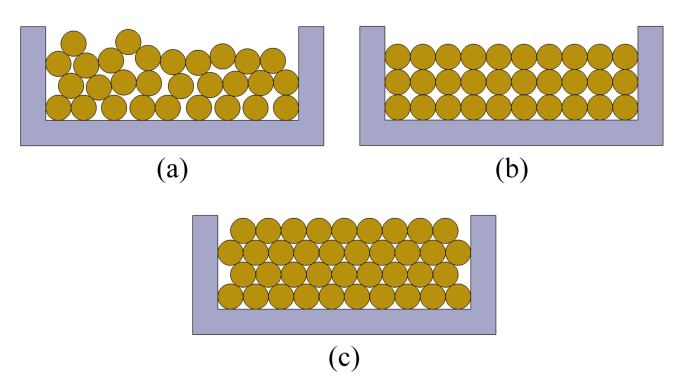


Fig. 6. (Color online) Comparison of conductor stacking patterns: (a) Random winding, (b) Layer winding, (c) Orthocyclic winding.

limited. Under such conditions, applying orthocyclic winding may lead to inconsistencies in the winding pattern, particularly in the end-turn region, where upper and lower layers are wound in opposite directions. This can result in misalignment and difficulty maintaining interlayer consistency [13]. Accordingly, this study adopts layer winding as the basis for turn estimation. This method reduces conductor interference, maintains positional consistency, and achieves a relatively high fill factor compared to random winding. In multilayer configu-

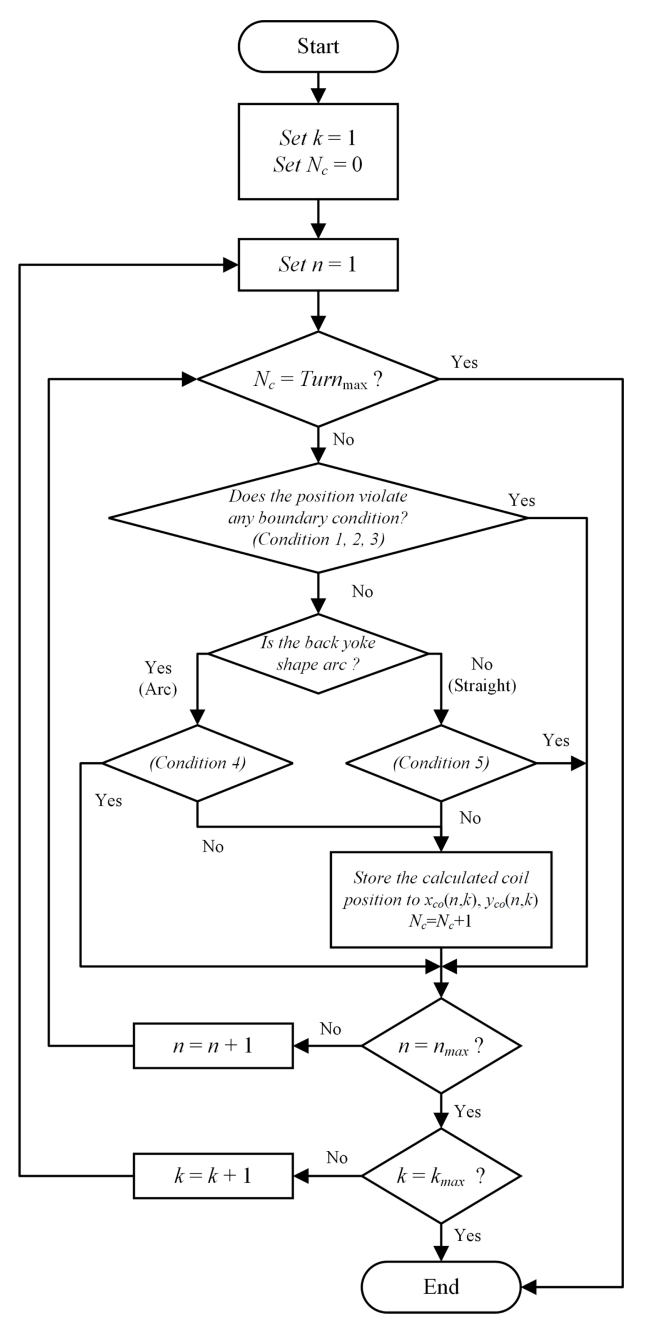


Fig. 7. Flowchart of the proposed turn estimation algorithm based on layer winding.

rations, layer winding ensures that upper-layer conductors are placed directly above the lower ones, without interference, even when winding progresses parallel to the tooth. It should be noted that the estimated turn count does not reflect the actual winding sequence. Rather, it represents a virtual configuration in which conductors are numbered from left to right and bottom to top. The overall procedure is summarized in Fig. 7, and the center coordinate of the first conductor is defined by Equation (10).

$$x_{co1} = x_{3is} + \frac{d_{co} + 2t_{co}}{2\sin\left(\frac{\theta_{sh}}{2} + \frac{\pi}{2N_s}\right)}\cos\left(\frac{\theta_{sh}}{2} - \frac{\pi}{2N_s}\right)$$
 (10.1)

$$y_{co1} = y_{3is} + \frac{d_{co} + 2t_{co}}{2\sin\left(\frac{\theta_{sh}}{2} + \frac{\pi}{2N_s}\right)} \sin\left(\frac{\theta_{sh}}{2} - \frac{\pi}{2N_s}\right)$$
(10.2)

At the end of the algorithm, the x- and y-coordinates of the center point P_{co} of each coil are calculated as shown in Equation (11).

$$x_{co}(n,k) = x_{co1} + (n-1)(d_{co} + 2t_{co})\cos\left(\frac{\pi}{N_s}\right) - \frac{(k-1)(d_{co} + 2t_{co})\cos(\pi - \theta_{sh})}{\sin\left(\pi - \left(\theta_{sh} + \frac{\pi}{N_s}\right)\right)}$$
(11.1)

$$y_{co}(n,k) = y_{col} + (n-1)(d_{co} + 2t_{co})\sin\left(\frac{\pi}{N_s}\right)$$

$$-\frac{(k-1)(d_{co} + 2t_{co})\sin(\pi - \theta_{sh})}{\sin\left(\pi - \left(\theta_{sh} + \frac{\pi}{N_s}\right)\right)}$$
(11.2)

To verify whether each generated coil position satisfies physical constraints, the algorithm defines five boundary conditions, as illustrated in Fig. 8. These conditions are formulated to ensure that winding placement remains within the permissible mechanical and geometric limits. If any condition is violated, the corresponding position is considered invalid.

Boundary Condition – 1: Violation of Inner Insulator Boundary

This condition checks whether the x-coordinate of the conductor exceeds the inner boundary of the insulator, defined as x_{2is} . If the position satisfies the inequality in

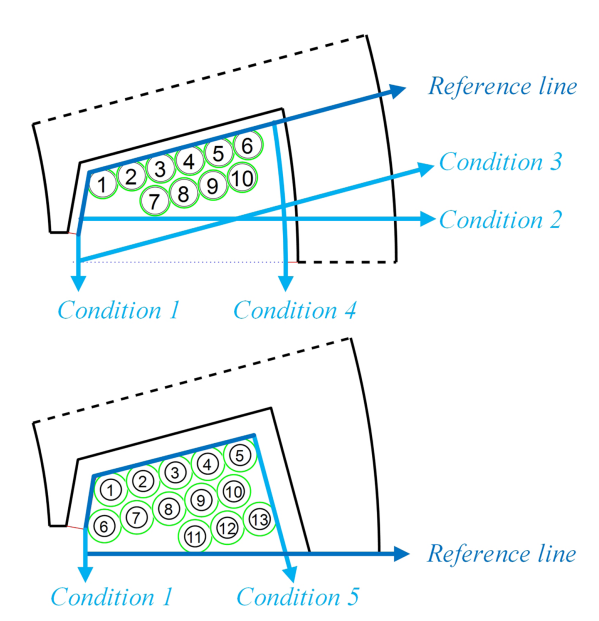


Fig. 8. (Color online) Boundary conditions for validating coil placement.

Equation (12), it lies outside the valid region.

$$x_{co} > x_{2is} + \frac{d_{co}}{2} + t_{co} \tag{12}$$

Boundary Condition – 2: Nozzle Interference (One-Piece Core)

This condition determines whether the *y*-coordinate of the conductor interferes with the winding nozzle in a one-piece core. If it exceeds the specified limit, the position is invalid, as expressed in Equation (13).

$$y_{co} > w_{oc} + \frac{d_{co}}{2} + t_{co} \tag{13}$$

Here, w_{oc} represents the thickness of the winding nozzle for the one-piece core configuration.

Boundary Condition – 3: Nozzle Interference (Connected Core)

For connected cores, the nozzle orientation differs from that of one-piece cores. Therefore, interference is evaluated using Equation (14)

$$y_{co} - x_{co} \tan\left(\frac{\pi}{N_s}\right) > \frac{2(w_{cc} + t_{co}) + d_{co}}{2\cos\left(\frac{\pi}{N_s}\right)} - r_{so} \tan\left(\frac{\pi}{N_s}\right)$$
 (14)

Here, w_{cc} denotes the nozzle thickness for the connected core configuration.

Boundary Conditions 2 and 3 define geometric con-

straints that are independent of slot geometry, such as slot opening width or tooth profile. Instead, these conditions are governed solely by nozzle thickness, allowing the constraints to be uniformly applied across different core types. These definitions ensure minimum mechanical clearance and prevent physical interference during winding insertion.

Boundary Condition – 4: Violation of Outer Back-Yoke Radius (Arc Type)

This condition verifies whether the conductor exceeds the outer radius of the back-yoke, r_{by} . If the distance from the coil center to the origin exceeds the threshold, the position is considered invalid. The corresponding expression is given in Equation (15).

$$\sqrt{x_{co}^2 + y_{co}^2} > r_{by} - t_{is} - \frac{d_{co}}{2} - t_{co}$$
 (15)

Boundary Condition – 5: Violation of Back-Yoke Line (Straight Type)

This condition applies when the back-yoke has a straight geometry. It checks whether the conductor exceeds a predefined linear boundary. This condition is applied selectively and mutually exclusively with *Boundary Condition 4*, depending on the back-yoke shape: arc-shaped cores use Condition 4, while straight-shaped cores use *Boundary Condition 5*. The inequality is defined in Equation (16).

$$y_{co} + \frac{x_{co}}{\tan\left(\frac{\pi}{N_s}\right)} > \frac{2(x_{4is} - t_{co}) - d_{co}}{2\cos\left(\frac{\pi}{N_s}\right)\tan\left(\frac{\pi}{N_s}\right)} + y_{4is}$$
(16)

The values of n_{max} and k_{max} are defined by Equation (17).

$$n_{max} = \left[\frac{r_{by} - x_{2is}}{(d_{co} + 2t_{co})\cos\left(\frac{\pi}{N_s}\right)} \right]$$
(17.1)

$$k_{max} = \left[\frac{y_{4is}}{(d_{co} + 2t_{co})\cos\left(\frac{\pi}{N_s}\right)} \right]$$
 (17.2)

5. Turn Estimation Results

Fig. 9 presents a comparison of stator slot geometries

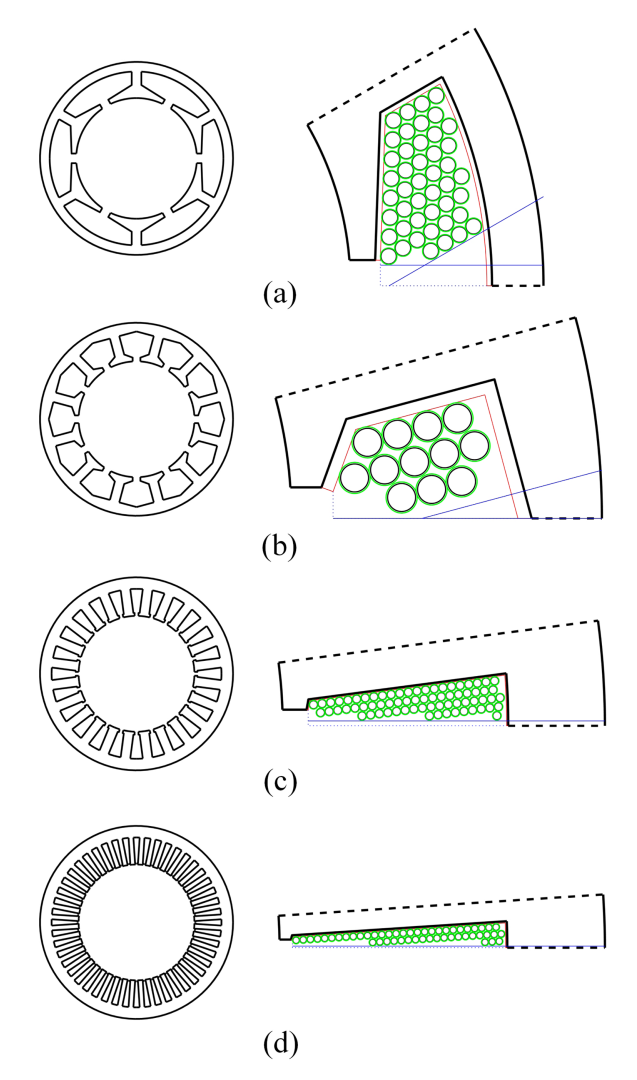


Fig. 9. (Color online) Comparison of stator slot geometries and winding configurations for different stator types: (a) 6-slot model with an arc-type back yoke, (b) 12-slot model with a straight-type back yoke, (c) 24-slot model with an arc-type back yoke, (d) 36-slot model with an arc-type back yoke.

and corresponding winding configurations for different stator types. The key design parameters used in each case are summarized in Table 1. These parameters were arbitrarily defined for the purpose of demonstrating the algorithm. For all combinations of the number of slots and back-yoke geometry, the conductor placement results were physically feasible without structural violations. These results confirm the general validity and applicability of the proposed algorithm to a wide range of practical stator designs.

Fig. 10(a) presents the predicted number of turns and coil arrangement obtained from the proposed algorithm, while Fig. 10(b) shows the actual core, insulator, and conductor layout based on the production drawing. The

Table 1. Design parameters and predicted number of turns used for the four stator models shown in Fig. 9.

Parameter -	Value			
	(a)	(b)	(c)	(d)
$r_{so}(\text{mm})$	100	50	500	500
$r_{si}(mm)$	62.5	30	300	300
$h_{so}(\mathrm{mm})$	5	2	15	7
$w_t(mm)$	5	2	10	5
N_s	6	12	24	48
$\theta_{sh}({ m Deg.})$	92	110	100	105
$r_{by}(mm)$	90	44	440	440
t_{is} (mm)	1	0.8	1	1
$d_{co}(\mathrm{mm})$	2	1.8	5	4
$t_{co}(\text{mm})$	0.1	0.1	0.2	0.2
w_{oc} (mm)	4	0	3	1
$w_{cc}(\text{mm})$	15	3	0	0
Back yoke shape	Arc	Straight	Arc	Arc
Predicted number of turns	45	12	72	51

manufactured motor adopts a connected core structure, and the insulator incorporates chamfers, fillets, and nonuniform features introduced during the injection molding process, as well as grooves intended to align the first layer winding. The target model used for verification is a three-phase, 14-pole, 12-slot electric motor designed for use in EV components. As shown in the Fig. 10(a), Boundary Condition 5, applied specifically for connected cores, was appropriately implemented in the turn estimation algorithm. The predicted number of turns, 21, precisely matches that of the fabricated machine. Although the algorithm assumes a layer winding scheme, while the actual motor was manufactured using an orthocyclic winding method, the predicted conductor placement exhibits strong geometric similarity. This result confirms the practical applicability and robustness of the proposed method.

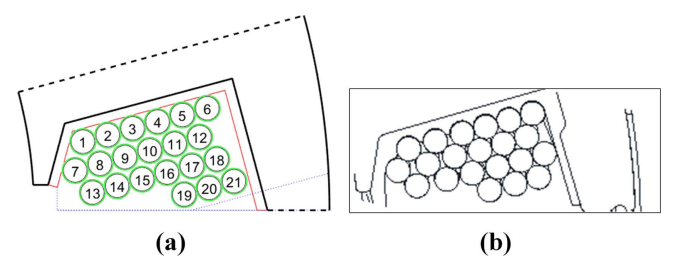


Fig. 10. (Color online) Comparison of predicted and actual coil layout: (a) Coil arrangement and turn count predicted by the proposed algorithm, (b) Actual core, insulator, and conductor layout from production drawing.

6. Conclusions

This study proposed a turn estimation algorithm that incorporates slot geometry and insulator constraints to accurately predict the number of winding turns in electric machines. While recent advancements in multicore parallel computing have enabled high-fidelity electromagnetic analysis that considers complex geometries and nonlinear magnetic characteristics, turn count and winding resistance are still typically determined manually. To address this limitation, the proposed method formulates key geometric parameters such as stator slot shape, insulator thickness, and coil diameter, all of which directly reflect actual manufacturing conditions. In addition, the algorithm accommodates geometric winding constraints associated with the three representative core manufacturing methods. The algorithm is based on a layer winding configuration with uniformly spaced conductors, and the number of turns is estimated by evaluating five geometric boundary conditions, thereby enabling flexible applicability across a wide range of design specifications. This enables a theoretical and quantitative approach to turn estimation rather than relying on empirical or experience-based methods.

This study demonstrates that the proposed method provides a reliable foundation for automating the design and optimization of electric machines. It estimates the maximum number of winding turns based on slot-level geometric constraints, offering early-stage design guidance under structural limitations. However, the method does not consider electromagnetic performance factors such as back-EMF, voltage drop, or current limits. These aspects require accurate resistance calculation, which depends on the three-dimensional geometry of the winding, including conductor length and layout. To address this limitation, future work will extend the algorithm to support threedimensional coil modeling and resistance estimation. This will enable more complete turn optimization that considers both mechanical feasibility and electrical performance under actual operating conditions. Due to confidentiality and industrial security concerns, detailed parameter values of the test model cannot be disclosed in this paper. However, the presented equations are provided with sufficient detail to allow the reproduction of similar winding structures and to derive comparable results when appropriate parameters are applied.

Acknowledgment

This research was financially supported by the Ministry of Trade, Industry and Energy, Korea, under the "Regional

Innovation Cluster Development Program (R&D, P0025293)" supervised by the Korea Institute for Advancement of Technology (KIAT).

References

- [1] H. Park, J. Yoon, J. Jung, H. Jung, and H. Yeo, Abstract Book of the Spring Conference of the KSAE 1137 (2019).
- [2] D. Kim, Y. Jung, K. Kim, and M. Park, J. Magn. 29, 259 (2024).
- [3] N. Gadiyar and B. Wang, IEEE ECCE, Detroit, MI, USA (2022).
- [4] J. Moon, D. Lee, and D. Kang, J. Magn. 27, 356 (2022).
- [5] S. Xu, D. Liu, and Z. Yao, J. Magn. 30, 19 (2025).
- [6] H. Qiu, Y. Zhang, K. Hu, C. Yang, and R. Yi, Energies 12, 2363 (2019).
- [7] D. Matt, N. Boubaker, M. Aitakkache, P. Enrici, J.-J.

- Huselstein, and T. Martire, New Perspectives on Electric Vehicles. IntechOpen, London (2022) pp. 1-23.
- [8] A. Mayr, F. Scheffler, R.t Fuder, T. Raffin, D. Kißkalt, and J. Franke, Procedia CIRP 118, 873 (2023).
- [9] M. Masoumi, K. Rajasekhara, D. Parati, and B. Bilgin, IEEE Access 10, 130212 (2022).
- [10] B.-K. Song, D.-K. Kim, S.-I. Kim, H.-J. Park, G.-H. Lee, and M.-S. Lim, IEEE Access 8, 167930 (2020).
- [11] W. Tong, Mechanical Design of Electric Motors, CRC Press, Florida (2014) pp. 219-225.
- [12] H. Akita, Y. Nakahara, N. Miyake, and T. Oikawa, 38th IAS Annual Meeting on Conference Record of the Industry Applications Conference 1, 367 (2003).
- [13] A. Mayr, D. Kißkalt, A. Lomakin, K. Graichen, and J. Franke, Procedia CIRP **96**, 80 (2021).
- [14] A. Dietz, A. O. Di Tommaso, F. Marignetti, R. Miceli, and C. Nevoloso, Energies 13, 1041 (2020).